Biomaterials and Biosystems 5 (2022) 100038

Contents lists available at ScienceDirect

Biomaterials and Biosystems

journal homepage: www.elsevier.com/locate/bbiosy

Magnetic $CuFe_2O_4$ with intrinsic protease-like activity inhibited cancer cell proliferation and migration through mediating intracellular proteins

Daomei Chen[a], Liang Jiang[a,b,c], Tao Lei[a,b,c], Guo Xiao[a,b,c], Yuanfeng Wang[a,b,c], Xiaoqiong Zuo[a,b,c], Bin Li[b,*], Lingli Li[a,b,c], Jiaqiang Wang[a,b,c,*]

[a] National Center for International Research on Photoelectric and Energy Materials, School of Materials and Energy, Yunnan University, Kunming 650091, P R China
[b] Key Laboratory of Medicinal Chemistry for Natural Resource, Ministry of Education, Yunnan University, Kunming 650091, P R China
[c] School of Chemical Sciences & Technology, Yunnan University, Kunming 650091, P R China

ARTICLE INFO

Keywords:
Magnetic nanomaterials
Protease-like activity
Cytotoxicity
MMP-2/9
F-actin
NF-*k*B

ABSTRACT

Protease has been widely used in biological and industrial fields. Developing efficient artificial enzyme mimics remains a major technical challenge due to the high stability of peptide bonds. Nanoenzymes with high stability, high activity and low cost, provided new opportunities to break through natural enzyme inherent limitations. However, compared with many nanomaterials with inherent peroxidase activity, the intrinsic mimic proteases properties of magnetic nanomaterials were seldom explored, let alone the interaction between magnetic nanomaterials and cellular proteins. Herein, we reported for the first time that magnetic $CuFe_2O_4$ possesses inherent protease activity to hydrolyze bovine serum albumin (BSA) and casein under physiological conditions, and the $CuFe_2O_4$ is more resistant to high temperature than the natural trypsin. It also exhibited significantly higher catalytic efficiency than other copper nanomaterials and can be recycled for many times. Protease participated in pathophysiological processes and all stages of tumor progression. Interesting, $CuFe_2O_4$ exhibited anti-proliferative effect on A549, SKOV3, HT-29, BABL-3T3 and HUVEC cells, as well as it was particularly sensitive against SKOV3 cells. $CuFe_2O_4$ was about 30 times more effective than conventional chemotherapy drugs oxaliplatin and artesunate against SKOV3 cells. In addition, $CuFe_2O_4$ also mediated the expression of intracellular proteins, such as MMP-2, MMP-9, F-actin, and NF-*k*B, which may be associated with global protein hydrolysis by $CuFe_2O_4$, leading to inhibition of cell migration. The merits of the high magnetic properties, good protease-mimic and antitumor activities make $CuFe_2O_4$ nanoparticles very prospective candidates for many applications such as proteomics and biotechnology.

1. Introduction

Natural enzymes are a type of biocatalyst that can accelerate one or a type of chemical reaction without sacrificing itself, which have important biological and industrial applications such as structural analysis of proteins, protein engineering technology and the design of protein cleavage drugs for specific targets [1,2]. However, the activity and stability of natural enzymes are highly dependent on the mild reaction conditions and environments due to their molecular structure, which dramatically hinder their practical application [3,4]. Great efforts have been devoted to developing artificial enzyme mimics to address these limitations. Many metal ion complexes as an artificial enzyme mimics, such as Cu, Co, Ni, Zn and Zr complexes, have been used for hydrolysis protein in the past few decades [5–11]. Although their selectivity and stability have been improved through connecting a binding site that recognizes the target protein to a catalytic group and cross-linking polystyrene, low catalytic efficiency and recovery is still a challenge [12,13].

Since Fe_3O_4 magnetic nanoparticle with intrinsic peroxidase-like activity has been reported by Yan and coworkers in 2007 [14], nanozymes have attracted extensive attention and related research has been growing exponentially. A variety of nanomaterials have been found to possess intrinsic enzyme mimic activities, such as transition metal oxides, chalcogenides, noble metals, and carbon-based nanomaterials, which were focused on peroxidase, oxidase, superoxide oxidase and catalase and so on. However, little attention has been paid to nanomaterials themselves in exploring their intrinsic protease-like activities. We reported Cu-MOF possesses highly efficient intrinsic protease-like activity and called it “MOFzyme”, which hydrolyzed the proteins including bovine serum albumin (BSA) and casein at alkaline solution (pH 9.0) and high temperature of 50–70 °C [15]. Tatjana N. Parac-Vogt and coworkers found MOF-808 and NU-1000 could be a stable and superior catalyst for peptide bond hydrolysis [1,2]. Recently, we found Cu_2O

* Corresponding authors.
E-mail addresses: libin36@ynu.edu.cn (B. Li), jqwang@ynu.edu.cn (J. Wang).

https://doi.org/10.1016/j.bbiosy.2021.100038
Received 1 July 2021; Received in revised form 29 December 2021; Accepted 30 December 2021

and carbon quantum dots (CQDs/Cu_2O) composite can hydrolyze BSA and casein under physiological conditions and the proteolytic activity was improved compared with MOFzyme [16]. Nanomaterials with high stability and low cost, as well as inherent physicochemical properties (magnetic, optical, thermal and electrical properties) and protease-like activities, will endow them with extensive potential compared to natural enzymes [3]. Nevertheless, the properties of magnetic nanomaterials that mimic proteases under physiological conditions have never been reported.

On the other hand, the proteases naturally expressed by living organisms have the ability to coordinate pathophysiological processes, even participated in all stages of tumor progression. For example, matrix metalloproteinases (MMPs) and cytoskeleton. MMPs are a family of enzymes proteolytically, especially gelatinases MMP-2 and MMP-9, providing opportunities for tumor invasion and metastasis through degrading the extracellular matrix (ECM) to remodeling of basement membranes and angiogenesis [17,18]. It is worth noting that the abnormal expression of MMP-2 is a prominent feature of epithelial ovarian tumorigenesis and the expression of MMP-9 can also cause the changes of trypsinogen isoenzyme levels in ovarian tumor cyst fluid [19,20]. Therefore, inhibition of tumor metastasis can be achieved by reducing the expression of MMP-2/9 in the tumor microenvironment or reducing their activity [17,21,22]. Unfortunately, only a few nanomaterials including Fe_3O_4 nanoparticles coated with piroctone olamine [23], hollow mesoporous carbon nanocapsules [24] and fullerene-based nanomaterial $Gd@C_{82}(OH)_{22}$ [25] have been found to possess inhibition of MMP-2/9 MMPs activity.

In various tumor cells, MMP-9 activity is tightly controlled by transcriptional level, involving nuclear factor-*k*B (NF-*k*B) [26]. NF- *k*B, a member of Rel transcription factor family, participates in the mediation of many biological activities including inflammation, immune response, cell proliferation, and apoptotic cell death. In most normal cells, NF-*k*B is retained in the cytoplasm as an inactive complex through the direct binding of an I*k*B inhibitor. Upon certain stimulations, I*k*B is rapidly phosphorylated and degraded, allowing NF-*k*B to translocate to the nucleus. The last few years have reported continuous activation of NF-*k*B factors is emerging as a hallmark of various types of solid tumors, including breast, ovarian, colon [27,28]. NF-*k*B activity is generally associated with the growth and migration of the tumor cells.

In addition, cytoskeleton maintained the structural integrity of cells also plays an impotent role in the regulation of tumor metastasis [29,30]. Recently, we reported Cu-MOF and CQDs/Cu_2O with protease-like activities affected cellular microenvironment and induced ovarian cancer SKOV3 cells death through mediating the expression of matrix metalloproteinases, angiogenic cytokines and cytoskeleton [30,31].

$CuFe_2O_4$, one of spinel ferrites with the general formula of MFe_2O_4 (M = Co, Ni, Cu, etc.), has been extensively exploited in applications including magnetism, catalysis, electronics and energy conversion due to rich redox chemistry, high electronic conductivity, good superparamagnetic properties, easy preparation and good stability. For example, $CuFe_2O_4/Cu_9S_8$ /PPy ternary nanotubes and Cu-$CuFe_2O_4$ were used as peroxidase mimics to detect H_2O_2 [32,33]. It has been found other spinel ferrites such as $CoFe_2O_4$, $ZnFe_2O_4$, $MgFe_2O_4$, $NiFe_2O_4$ nanoparticles and their composites, also exhibit peroxidase-like activity and are used for relevant determinations by redox interaction [34–37]. Pt/$CoFe_2O_4$ and MoS_2@$CoFe_2O_4$ nanoparticles with peroxidase-like activity were used to detect dopamine, cysteine and glutathione [36,37]. Compared with other spinel ferrites, $CuFe_2O_4$-base nanoparticles showed excellent peroxidase-like activity, which possesses stronger affinity to H_2O_2, and even better than nature horseradish enzyme (HRP) [33]. On the basis of our previous research results, the nanomaterials containing copper, such as Cu-MOF, CQDs/CuO_2, showed good protease-like activity. However, the inherent protease-like properties of these magnetic nanomaterials have not been explored, let alone the interaction between magnetic nanomaterials and cellular proteins.

In this study, we showed the first magnetic protease mimic, $CuFe_2O_4$ has an inherent protease activity. Moreover, the effect of $CuFe_2O_4$ on proliferation and migration-relative proteins including MMP-2/9, NF-*k*B and F-actin were also studied. The stability, simple synthesis, easy separation and versatility of $CuFe_2O_4$ nanoparticles make them a powerful tool for a wide range of potential applications in medicine and biotechnology. It would provide a new insight into the relationship between intracellular protein and magnetic materials, and show a promising prospect in tumor therapy.

2. Materials and methods

2.1. Chemicals and instrumentation

Copper dichloride dihydrate ($CuCl_2$• $2H_2O$, 99%), NaOH, polyethylene glycol (PEG, 99%), sodium acetate (NaAc), ferric chloride hexahydrate ($FeCl_3$•$6H_2O$, 99%), ethanol, casein, bovine serum albumin (BSA) were acquired from Sigma-Aldrich. Streptomycin and Penicillin were acquired from Sigma Chemical Co. Ltd., (St. Louis, MO, USA). Dimethyl sulfoxide (DMSO) was obtained from Yongda Chemical Reagent Co., Ltd. (Tianjin, China). Fetal bovine serum and DMEM medium were purchased from Hyclone Laboratories (Logan, UT). The powder synchrotron X-ray diffraction patterns were obtained on a Cu Kα radiation in a 2θ range 20–80° using a D/max-3B spectrometer. Scanning electron microscopy (SEM) images of samples were visualized using a FEI Quanta 200FEG microscope. Transmission electron microscopy (TEM) images of samples were performed on a JEM-2100 microscope. BET surface areas, pore volumes and Pore size distributions were carried out through nitrogen adsorption/desorption measurements using a Micromeritics Tristar II surface area and porosity analyzer. The cells were analyzed using an Olympus IX73 fluorescent microscope (Olympus IX73, Japan) and a FACSCalibur flow cytometer (Becton Dickinson, San Jose, CA.). Images of the western blot were taken with the Champchemi Professional image analysis system (Sagecreation, Beijing, China).

2.2. Synthesis of $CuFe_2O_4$

$CuFe_2O_4$ was synthesized with copper dichloride dihydrate, ferric chloride hexahydrate based on reported works [38, 39]. Simply, $CuCl_2$•$2H_2O$ (0.170 g) and $FeCl_3$•$6H_2O$ (0.54 g) were dissolved in 40 mL ethylene glycol, stir well until the solution is clear and no related precipitation, anhydrous sodium acetate (3.6 g) and polyethylene glycol (1 g, M = 20,000) add it to the above solution and stirred overnight. And after that, it was transfer to an autoclave with Teflon lining for reaction (10 h, 200 °C). After cooling, the product in the reaction mixture was centrifuged and washed (5 times in ethanol and water) until the product was pure. Finally, in the oven for 6 h at 60 °C to obtain pure $CuFe_2O_4$.

2.3. Proteolysis reactions

A certain amount of $CuFe_2O_4$ was added in the reaction solution (total volume: 10 mL) that consisted of phosphate buffer solution (pH 7.4) and BSA or casein (10 mg). The hydrolysis reaction of $CuFe_2O_4$ activity was carried out under the different temperatures (37, 50 and 70 °C) and the time from 0 to 60 min, the shaking speed (180 rpm) provided by isothermal water bathing shaking apparatus. 1 mL of the reaction mixture was taken out at regular intervals. In this experiment, the buffers (50 mM) we used were boric acid-sodium borate buffer solution (pH 8.0~10.0) and phosphoric acid-sodium phosphate buffer solution (pH 7.4). Before use, filter all buffers through a 0.45 mm microporous filter. We use a higher precision pH meter to measure pH. The protein solution stored at −20 °C. Separate the solid complex from the peptide solution by a magnet. Use BSA solution without $CuFe_2O_4$ as the control group. After reaction, the hydrolysate was separated by polyacrylamide gel electrophoresis (SDS-PAGE) and conducted according to

the literatures [11,13]. Simply, the protein sample was mixed with SDS-PAGE loading buffer. 10 μg protein was separated by a 4%–12% SDS-PAGE gel, and the standard protein ladder was used as the reference for molecular weights (MWs). Electrophoresis was performed using a electrophoresis system (Cleaver Scientific Ltd, United Kingdom) at constant voltage (100 V). Gels were stained using 0.10% solution of Coomassie Brilliant Blue G-250 in an aqueous solution that contained 10% of acetic acid and 40% of methanol for 1 h at room temperature. Washed with ethanol and acetic acid and scanned using Epson perfection V33. The intensity of the band corresponding to the protein was determined by an Alpha View SA model. The rate of protein hydrolysis was measured by monitoring the decrease in the intensity of the electrophoretic bands, then obtained initial rate plots by analyzing the data. Measuring the kinetic data at different C_0 (0~3 mM) and different temperature (37 °C, 50 °C, 70 °C) at the optimum pH 7.4. Estimating the pseudo-first-order kinetic constants (k_0) according to a logarithmic plot, k_0 = -ln[S]/$[S]_0$, which $[S]_0$ meant the primary protein concentration and [S] represented the concentration of protein that was estimated at a specified time point.

2.4. Reusability of $CuFe_2O_4$

In order to verify the stability of the material, the following experimental program was adopted: the catalytic hydrolysis reaction was placed in an environment of 37 °C and pH 7.4. 10 mg $CuFe_2O_4$ was added to BSA solution (15 μM). After 30 min, taking out hydrolysate (1 mL) from the reaction solution and the catalyst was recollected with a magnet and washed for three times with ethanol and water, respectively, to remove amino acid left and peptide fragments. Analyzing the protein in transparent liquid via SDS-PAGE. Removed solvent under vacuum (6 h, 60 °C). Recovery experiment was conducted after each hydrolyzing reaction. The experiment went through eight cycles. The rate of proteolysis was analyzed by measuring reduce in electrophoretic band intensity. The effect of $CuFe_2O_4$ recycling is expressed as relative activity.

2.5. Cancer cell line and culture

Human ovarian cancer cells (SKOV3), human colon cancer cell cells (HT-29), human lung adenocarcinoma cells (A549), human umbilical vein endothelial cells (HUVECs), and Mouse embryonic fibroblasts cells (BABL-3T3) were purchased from shanghai life science of chinese academy of sciences. BABL-3T3 cells were cultivated in high-glucose Dulbecco's modified Eagles medium (DMEM) and other cells were cultivated in low glucose DMEM for 24–72 h, the low glucose DMEM contained 1% penicillin/streptomycin (P/S, Boster) and 10% fetal bovine serum (FBS), HUVECs were incubated with DMEM containing 20% FBS. Culture all cells in a humidified incubator (5% CO_2, 37 °C).

2.6. Cytotoxicity assay in vitro

The cytotoxicity of $CuFe_2O_4$ was measured by the MTT assay using four cell lines (A549, HT-29, HUVEC, and SKOV3) and with BABL-3T3 cells as control. SKOV3, A549, HUVEC, BABL-3T3 and HT-29 cells were seeded in 96-well plates at the density of 2×10^4 cells per well containing normal growth medium. After 24 h of culture at 37 °C, using different concentrations of $CuFe_2O_4$ (0.78–12.5 μg mL^{-1}) to incubate cells for 24, 48 and 72 h. After that, MTT solution (5 μg mL^{-1}, 50μL) was added to each tested wells, followed by incubation for 4 h. Remove all media and added 150μL DMSO to the wells. Measure the absorbance of each sample at 490 nm by microplate reader. The number of cells was obtained as absorbance values. The inhibition rate (%) $= \frac{[OD]control-[OD]test}{[OD]control-[OD]BL}$, where $[OD]_{BL}$ is the average absorbances of the wells which without anything added, $[OD]_{test}$ and $[OD]_{control}$ are the average absorbances of the test samples and control, respectively. The results were expressed as IC_{50} values and the results were averaged. All experiments were repeated at least three times.

2.7. Apoptosis assay by AO/EB staining

Inoculate the separated SKOV3 cells into a 35 mm culture dish (2×10^5 cells/dish), and then cultured with different concentrations of $CuFe_2O_4$ (0, 3.12, 6.25, 12.5 μg mL^{-1}) for 24 h. Collect cells by centrifugation, after washed with 2 mL of PBS for three times, cells were incubated with AO/EB (5 μg mL^{-1}) for 6 min and then placed the cover slips on glass slides to examine the cells by a confocal fluorescence microscopic system.

2.8. Analysis of apoptosis by flow cytometry

Inoculate the separated SKOV3 cells into a 35 mm culture dish (2×10^5 cells/dish), and then cultured with different concentrations of $CuFe_2O_4$ (0, 3.12, 6.25, 12.5 μg mL^{-1}) for 24 h. Digested with trypsin, collected cells by centrifugation (1×10^6), washed three times with PBS in an ice bath, added 1 mL 70% ethanol to the cells and fixed for 24 h. Stained with FITC-Annexin-V and PI dyes at room temperature and avoided light for 20 min. The FACSC alibur flow cytometer was used to measure the fluorescence emission at 490 nm. At least 1×10^4 cells were counted for each sample.

2.9. Effects of $CuFe_2O_4$ on migration of SKOV3 cells

SKOV3 cells were seeded in a 6-well plate (2×10^5 cells /well) for 24 h. The monolayer of cells were scraped in a straight line with the pipette tip, washed the non-adherent cells away with PBS, and added fresh medium and $CuFe_2O_4$ (0, 3.12, 6.25, 12.5 μg mL^{-1}). Microscopic photographs were taken after cultured for 0, 6, 12, and 24 h, respectively, to observe the number of cells migrating to the scratches and repeated each experiment for three times.

2.10. Western blot

Inoculate the separated SKOV3 cells into a 35 mm culture dish (2×10^5 cells/dish), and culture them for 24 h. Next, $CuFe_2O_4$ was added at a different concentration (0, 3.12, 6.25, 12.5, 25 μg mL^{-1}), and the control group was added no material. After 24 h, cells were isolated and harvested by centrifugation for 5 min at 1000 rpm. Then, lysis buffer (150 mM NaCl, 20 mM Tris–HCl, 1 mM PMSF, EDTA, leupeptin, 1% Triton X-100, SDS and 10% β-mercaptoethanol) was added and centrifuge the lysed cells (4 °C, 14000r/min, 15 min). Separated proteins via 10% SDS-PAGE, moved it to PVDF membranes according to standard process. Next, it was blocked with a buffer including 0.05% Tween-20 (polyoxyethy-lene-20 sorbitan monolaurate) and 5% skimmed milk at 4 °C, and then membranes were cultured for 1 hour with primary antibody(GAPDH 1:3000, MMP-2/9 1:200, NF-kB: 1:200, F-actin:1:200) at room temperature. Wash the membrane three times with PBST, add secondary antibody and incubate for 1 h after washing. Then the membrane were treated chemiluminescence agents. Images were taken with the Champchemi Professional image analysis system.

3. Results

3.1. Characterizations of $CuFe_2O_4$

Crystalline structures of the synthesized $CuFe_2O_4$ were confirmed with powder XRD measurements (Fig. S1) (**Supporting Information**). Figure S1 shows that the diffraction peak of $CuFe_2O_4$ is consistent with the product synthesized in the literature [38], where diffraction peaks at 18.3°, 32.0°, 35.7°, 43.3°, 53.6° and 74.3° are correspond to the (111), (220), (311), (400), (422) and (533) planes of $CuFe_2O_4$ (JCPDS no: 77–0010). SEM images shows that the $CuFe_2O_4$ particles are agglomerate, which may be mainly due to the fact that the material itself has strong magnetic properties and the particles are relatively small (Fig. 1A,B). The HRTEM image shows uniform spherical particles of 5–10 nm in

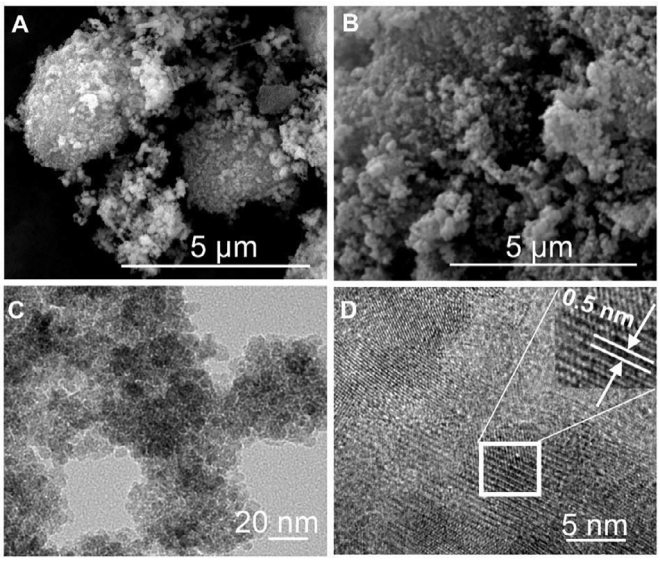

Fig. 1. (A, B) SEM images of the $CuFe_2O_4$. (C, D) TEM and HRTEM images of the $CuFe_2O_4$.

diameter with protruding nanostructures (Fig. 1C), and displayed the lattice spacing to be 0.502 nm, which corresponds exactly to the D-spacing of the (111) planes of $CuFe_2O_4$ (Fig. 1D). The nitrogen adsorption/desorption isotherm of $CuFe_2O_4$ is of type III and which is the inverse Langmuir curve (Fig. S2) and the specific surface area of $CuFe_2O_4$ is 135 $m^2\ g^{-1}$. The above mentioned results suggest that $CuFe_2O_4$ was successfully synthesized.

3.2. Protease-like activity of $CuFe_2O_4$

We measured the protease-like activity of $CuFe_2O_4$ used BSA as a substrate by changing the values of pH (5.5 to 9.0) and temperature (37 °C to 70 °C). When $CuFe_2O_4$ was added to a buffer solution including a protein substrate, we examined the effect of hydrolyzing protein via SDS-PAGE. In order to confirm that the disappearance of the BSA electrophoretic band is not caused by the adsorption of the catalyst, we measured the total amino acid content before and after the reaction. pH and temperature are important factors that must be considered in protein hydrolysis. As shown in Figure S3, the optimum pH was 7.4. Therefore, the proteolytic experiment was carried out under neutral conditions.

Under the condition of 37 °C and pH 7.4, the decrease of the BSA band intensity within 60 min was observed, suggesting $CuFe_2O_4$ possess the ability to hydrolyze BSA and the hydrolytic activity of $CuFe_2O_4$ was very weak under this condition (Fig. 2A). The intensity of the BSA band decreased significantly after 60 min at 50 °C (Fig. 2B) . When temperature was raised to 70 °C, the most of BSA bands disappeared after 12 min, indicating the activity of $CuFe_2O_4$ increased sharply at 70 °C (Fig. 2C).

The effect of $CuFe_2O_4$ on hydrolysis of BSA was compared with trypsin. As shown in Fig. 2D, a series of small protein fragments hydrolyzed by nature trypsin were observed in the SDS-PAGE (with the molecular weights of ≈ 55, 40, 35 and 30 kDa). However, the amount of BSA decreases but no obvious smaller protein fragments appeared at the SDS-PAGE gels after $CuFe_2O_4$ treatment, which may be due to the fact that the $CuFe_2O_4$ hydrolyzed BSA into smaller fragments that cannot be observed on gels. When the molar ratio of $CuFe_2O_4$ vs. BSA was 10, BSA incubated with $CuFe_2O_4$ for 6 h, 12 h and 24 h at 50 °C, three small protein fragments with the molecular weights of ≈ 50, 37 and 30 kDa were observed in the SDS-PAGE (Fig. S4). The results of MALDI-TOF MS shows that $CuFe_2O_4$ can hydrolyze BSA into smaller fragments with m/z of 9317.6, 8924.9, 8447.6 and 8123.1 after $CuFe_2O_4$ treatment at 37 °C (Fig. S5–7), even more protein fragments with m/z of 2013.2, 1884.2 and 1756.7 appeared at 70 °C. Therefore, it was further demonstrated $CuFe_2O_4$ can hydrolyze of BSA into smaller fragments.

The activity of $CuFe_2O_4$ hydrolyzing BSA increased as the increase of temperature, but there was little change after trypsin treatment for 12 min at 70 °C, which is probably due to deactivation of trypsin under high-temperature. The above result suggested the ability of $CuFe_2O_4$ to hydrolyze BSA into smaller fragments and is more resistant to high temperature than the natural trypsin.

3.3. Kinetic analysis

The steady-state kinetics were applied to explore the catalytic mechanism of $CuFe_2O_4$. A typical Michaelis-Menten curve was observed over the range of $CuFe_2O_4$ concentrations considered (Fig. S8). In order to obtain the vital kinetic parameters, we used nonlinear regression equation to analyze the data. Calculating the optical density of the substrate protein band at different temperatures to obtain the first-order rate constant k_0 (37 °C~ 70 °C). We calculated the k_o of BSA hydrolyzed by $CuFe_2O_4$ based on the curve of ln $[S]/[S]_0$ against time, as shown as Figure S8 A, C, E. At the optimum reaction condition, k_o reached $19.53 \times 10^4\ s^{-1}$. At 37, 50, 70 °C and pH 7.4, the initial concentration of $CuFe_2O_4$ were able to affect the k_o and the results were shown in Figure S8 B, 3D and 3F.

When the $CuFe_2O_4$ concentrations were lower, the hydrolysis rate was agreed with the first-order reaction kinetics. However, the curve performed a saturation trend when $CuFe_2O_4$ concentration was higher, suggesting that the Michaelis–Menten reaction mechanism (Eq. (1)) was abided by the catalytic hydrolysis of BSA. When $C_0 \gg [CS]$, pseudo-first-order kinetic behavior was predicted Eq. (2). According to the following formula, we can compute the kinetic parameters.

$$C + S \underset{k_{-1}}{\overset{k_1}{\rightleftharpoons}} CS \xrightarrow{k_2} C + P \tag{1}$$

$$k_0 = k_{cat} C_0 / (K_m + C_0) \tag{2}$$

$$k_{cat} = k_2 \tag{3}$$

$$K_m = (k_{-1} + k_2)/k_1 \tag{4}$$

*K*m, the Michaelis constant, defined as the affinity of the enzyme to its substrate. The value of *K*m is smaller; the affinity between the enzyme and the substrate is stronger. As shown in Table 1, BSA was hydrolyzed by $CuFe_2O_4$ under the optimum conditions; the K_m value of $CuFe_2O_4$ was about 4.5 times lower than the K_m value of CQDs/Cu_2O, and slightly lower than Cu-MOF under physiological conditions, but much lower than the composites of synthetic metlloproteinase Cu (II) at alkaline solution (pH 9.5) in Table 1.

Furthermore, the k_{cat} and k_{cat}/K_m usually measure catalytic activity directly. The derived k_{cat} of $CuFe_2O_4$ showed a value of $(4.43\pm0.26) \times 10^{-4}\ s^{-1}$ and $(8.77\pm0.38) \times 10^4\ s^{-1}$ and $(19.64\pm0.85) \times 10^4\ s^{-1}$ at the temperatures of 37 °C, 50 °C, and 70 °C respectively. The K_{cat} value of $CuFe_2O_4$ is significantly higher and is about 102-fold higher than Cu (II) oxacyclen. Although the k_{cat} of $CuFe_2O_4$ at 70 °C is lower than that of Cu-MOF ($20.98 \times 10^4\ s^{-1}$), Cu-MOF can only hydrolyze BSA under alkaline condition (pH 9.0), while $CuFe_2O_4$ can hydrolyze BSA at pH7.4, indicating that the condition for hydrolysis of proteins by $CuFe_2O_4$ is milder than that of Cu-MOF. The k_{cat} of $CuFe_2O_4$ is slightly higher than CQDs/Cu_2O.

In addition, the value of k_{cat}/K_m for BSA hydrolysis by $CuFe_2O_4$ at 50 °C and pH 7.4 is about 110-fold and greater than that by Cu(II)oxacyclen at 50 °C and pH 9.5. It is also much higher than the value of k_{cat}/K_m of CQDs/Cu_2O. The above mentioned results indicated that the affinity of the $CuFe_2O_4$ to the substrate is stronger than that for trypsin and majority of the synthetic metalloprotease Cu(II) composites and $CuFe_2O_4$ has a higher catalytic activity.

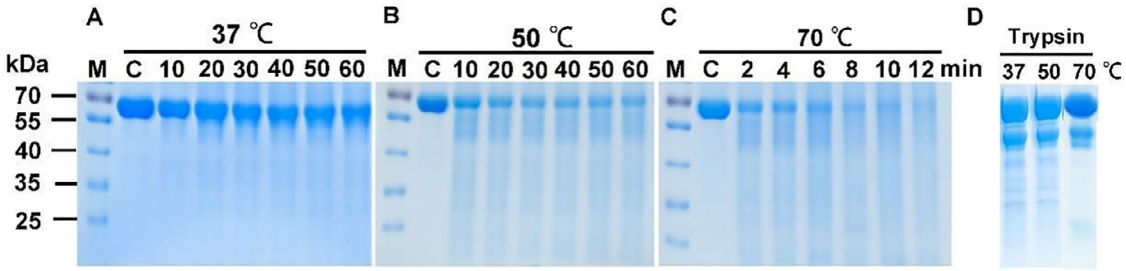

Fig. 2. SDS-PAGE of the hydrolyzed products of BSA (15 μM) by $CuFe_2O_4$ (3.0 mM) and trypsin (BSA: trypsin = 40:1 w/w) at pH 7.4. (A-C) $CuFe_2O_4$ and BSA reacted different times at 37 ˚C, 50 ˚C, 70 ˚C, respectively, M: Mark. C: BSA solution (without $CuFe_2O_4$) as the control groups. (D) BSA incubated with trypsin for 30 min at 37, 50 ˚C, and reacted 70 ˚C for 12 min.

Table 1
Comparison of various materials kinetic parameters of protein hydrolyze.

Catalyst	Protein	pH	T(˚)	*Km* (*10*$^{-}$3 M)	k_{cat}(10^{-4} s^{-1})	k_{cat}/ *Km*(s^{-1} M^{-1})	Refs
$CuFe_2O_4$	BSA	7.4	37	0.38±0.04	4.43±0.26	1.16±0.15	This work
$CuFe_2O_4$	BSA	7.4	50	0.22±0.02	8.77±0.38	3.98±0.20	This work
$CuFe_2O_4$	BSA	7.4	70	0.17±0.66	19.64±0.85	11.55±0.43	This work
$CuFe_2O_4$	Casein	7.4	50	0.74±0.25	3.95±0.16	0.53±0.20	This work
$CuFe_2O_4$	Casein	7.4	70	0.44±0.13	7.65±0.31	1.73±0.22	This work
CQDs/Cu_2O	BSA	7.4	37	0.93±0.24	3.95±0.14	0.42±0.19	[16]
CQDs/Cu_2O	BSA	7.4	50	0.79±0.15	5.36±0.19	0.67±0.17	[16]
CQDs/Cu_2O	BSA	7.4	70	0.72±0.18	16.93±0.32	2.35±0.25	[16]
CQDs/Cu_2O	Casein	7.4	50	0.45±0.12	5.56±0.39	1.23±0.25	[16]
CQDs/Cu_2O	Casein	7.4	70	0.26±0.06	10.78±1.17	4.14±0.61	[16]
Cu-MOF	BSA	9.0	50	0.28±0.04	6.28±0.39	2.23±0.35	[15]
Cu-MOF	BSA	9.0	70	0.27±0.02	20.98±0.65	7.73±0.68	[15]
Cu-MOF	Casein	9.0	50	1.16±0. 24	5.17±0.56	0.44±0.09	[15]
Cu-MOF	Casein	9.0	70	0.42±0.02	9.76±0.17	2.32±0.12	[15]
Cu(II)A-PS	BSA	9.5	50	0.92	8.00	0.87	[13]
Cu(II)B-PS	BSA	9.5	50	1.20	8.70	0.73	[13]
Cu(II)-oxacyclen	BSA	9.5	50	0.51±0.03	0.19±0.003	0.036±0.003	[40]
Cu(II)C	BSA	9.5	50	0.11±0.03	3.89±0.56	3.61±0.83	[11]
Cu(II)D	BSA	9.5	50	0.52±0.1	2.77±0.277	0.56±0.11	[11]
Cu(II)E	BSA	9.5	50	0.17±0.03	1.89±0.17	1.14±0.19	[11]
Cu(II)H	BSA	9.5	50	0.42±0.06	0.14±0.04	0.310±0.083	[11]

3.4. $CuFe_2O_4$ catalyzed hydrolysis of casein

The development of artificial proteases with hydrolytic activity for a wide range of substrates remains a major challenge. Casein is slightly soluble in water and acidic media and does not damage the structure even at a pressure of 100 MPa and a temperature of 100 ˚C, indicating it is difficult to be hydrolyzed. Herein, casein was selected as a substrate to test the proteolytic activity of $CuFe_2O_4$ (Fig. S9). As can be seen from Table 1, the k_m of casein hydrolyzed by $CuFe_2O_4$ were 0.74×10^{-3} M^{-1} and 0.44×10^{-3} M^{-1} at 50 ˚C, 70 ˚C, respectively, indicating that casein could also be hydrolyzed by $CuFe_2O_4$. When the reaction conditions are the same, the values of k_{cat}/K_m are 0.53 $s^{-1}M^{-1}$ at 50 ˚C and 1.78 $s^{-1}M^{-1}$ at 70 ˚C for casein, which are about 8 times and 7-fold lower than that for BSA (3.98 s^{-1} M^{-1} at 50 ˚C and 12.1s^{-1} M^{-1} at 70 ˚C), suggesting casein is more difficult to be hydrolyzed than BSA. Although the k_{cat} and k_{cat}/ *Km* of $CuFe_2O_4$ are slightly lower than that of Cu-MOF and CQDs/Cu_2O nanocomposites, $CuFe_2O_4$ as the first magnetic nanomaterial exhibits high potency to mimic protease activity and hydrolyze proteins under neutral conditions. Considering energy consumption and cost, $CuFe_2O_4$ is more suitable for a large number of industrial production applications.

3.5. Reusability

$CuFe_2O_4$, as a novel mimic protease, could also be treated as an effective heterogeneous proteolytic material. As shown in Figure S10, we can easily separate it from the reaction solution by a magnet and repeatedly use it, this is one of the most prominent advantages compared to natural enzymes and other nanomaterials. The reusability of $CuFe_2O_4$ is outstanding and after eight cycles of use, its activity did not decrease remarkably, and still maintained 87% of its primary activity (Fig. S11). It can be seen from XRD patterns of $CuFe_2O_4$ before and after reacted with BSA solution at 30 min at pH 7.4, 37 ˚C, that the crystal shape of $CuFe_2O_4$ hardly changed, revealing that $CuFe_2O_4$ was stable during the reaction (Fig. S12). Thus, $CuFe_2O_4$ performed a superior stability and it could be treated as an effective heterogeneous proteolytic catalyst.

3.6. Effect of $CuFe_2O_4$ on cell growth

We used the MTT assay to evaluate the cytotoxicity of $CuFe_2O_4$ in five cell lines, including human lung adenocarcinoma cells (A549), human ovarian cancer cells (SKOV3), human colorectal cancer cells (HT-29), normal human umbilical vein endothelial cells (HUVECs), normal mouse embryonic mouse embryonic fibroblast cells (BABL-3T3). As shown in Figure S13, $CuFe_2O_4$ displayed concentration-dependent inhibition in all tested cells, and possesses highest inhibition rate against SKOV3. The inhibition rate against SKOV3 reached 60% after treated by 12.5 μg mL^{-1} $CuFe_2O_4$ for 24 h, whereas the inhibition rate of HUVECs and BABL-3T3 was about 45% and 28%, respectively. The half maximal inhibitory concentration (IC_{50}) of A549, SKOV3, HT-29, BABL-3T3, HUVEC cells was 27.2, 8.3, 15.9, 25.9, 14.3 μg mL^{-1} respectively at 24 h (Fig. S13A and Table S1). The IC_{50} of $CuFe_2O_4$ against SKOV3 cells was the lowest among all the tested cells, and it was approximately 3-fold higher than normal BABL-3T3 cells. Moreover, $CuFe_2O_4$ was more toxic than commercially available chemother-

apy drugs, oxaliplatin (OXA) and artesunate (ART), the IC_{50} of OXA and ART against SKOV3 cells was 241.5 and 280.8 $\mu g\ mL^{-1}$ respectively at 24 h, which was higher than the IC_{50} of $CuFe_2O_4$ about 30 times. The results suggested the $CuFe_2O_4$ was particularly sensitive against SKOV3 cells.

3.7. $CuFe_2O_4$ induces apoptosis of SKOV3

We observed the nuclear morphology of $CuFe_2O_4$ treated cells and control cells by staining cell nuclei with AO/EB to further study the underlying mechanism of $CuFe_2O_4$ activity. After AO and EB staining, the surviving cells showed green fluorescence, the apoptotic cells were orange-red fluorescence. As shown in Fig. 3A, the control cells untreated $CuFe_2O_4$ were uniformly green. SKOV3 cells were treated with different concentrations of $CuFe_2O_4$ (3.12, 6.25 and 12.5 $\mu g\ mL^{-1}$) for 24 h, a number of cells with orange-red fluorescence were appeared and the number of this type cells was increased with the increase of material concentration, suggesting $CuFe_2O_4$ induced SKOV3 cells apoptosis. In addition, Annexin-V-FITC assay was performed to test cell apoptosis (Fig. 3B). In the two-parameter dot plot, the four quadrants represent living cell populations (lower left quadrant), early stage apoptotic cell groups (lower right quadrant), dead cells (upper left quadrant) and apoptotic cells that undergo secondary necrosis at the final stage (upper right quadrant). When the concentration of $CuFe_2O_4$ increased from 3.12 to 6.25 $\mu g\ mL^{-1}$, the proportion of last stage apoptotic cells increased from 17.4% to 38.8% and the proportion was much larger compared with the control group, but the proportion of upper left quadrant cells were not changed. The above results confirmed that $CuFe_2O_4$ is able to effectively induce the apoptosis of SKOV3 and mainly cause the last stage apoptosis of cells.

3.8. Effect of $CuFe_2O_4$ on migration of SKOV3

Cell migration is the basis of the life cycle of the organism, and it is also complex process that acts as an extremely considerable role in the course of tumor cell metastasis. Scratch method is one of the methods for determining the migration activity of drugs on tumor cells in vitro. We carried out scratch experiments and counted the number of cells that migrated to the scratch district after treating SKOV3 cells with different concentration of $CuFe_2O_4$ (3.12, 6.25 and 12.5 $\mu g\ mL^{-1}$) (Fig. 4A). The group without $CuFe_2O_4$ was used as a control group. As shown in Fig. 4B, the number of migrated cells was increased with the prolonging reaction time in control group, as well as the width of scratch became smaller. When treated with different concentration $CuFe_2O_4$, the migration inhibition rate was increased from 32.1 to 81.4%, the number of migrated cells was reduced sharply, suggested that $CuFe_2O_4$ possessed the ability to inhibit the migration of SKOV3.

3.9. Effect of $CuFe_2O_4$ on MMP-2/9 in SKOV3

The metastasis and invasion of tumor cells is a complex process involving many proteins. Matrix metalloproteinases (MMPs), especially gelatinases MMP-2 and MMP-9, promoting tumor metastasis and invasion by hydrolyzing cell basement membranes. Cytoskeleton F-actin and NF-*k*B are also associated with the growth and migration of the tumor cells. We found $CuFe_2O_4$ possessed intrinsic protease-like activity and has the significant effect on inhibiting SKOV3 cells growth and migration. Whether the protease-like activity of $CuFe_2O_4$ affects tumor proliferation and migration? We investigated the effect of $CuFe_2O_4$ on migration-relative proteins including MMP-2/9, NF-*k*B and F-actin. As shown in Fig. 4C and Figure S14, the expression of MMP-2, MMP-9, NF-*k*B and F-actin in SKOV3 cells decreased with the increase of the concentration of $CuFe_2O_4$. When treated by 12.5 $\mu g\ mL^{-1}$ $CuFe_2O_4$, the data of relative densitometric analysis showed a significant difference compared with control group ($P < 0.01$). Thus, $CuFe_2O_4$ could inhibit the activity of MMP-2, MMP-9, NF-*k*B and F-actin. Downregulation of MMP-2/9, F-actin and NF- *k*B proteins may be caused by global protein hydrolysis upon $CuFe_2O_4$ treatment, leading to inhibition of cell migration.

4. Discussion

Artificial enzymes have attracted much attention, because natural protease has the disadvantages of instability and low activity. Developing efficient artificial enzyme mimics remains a major technical challenge due to the high stability of peptide bonds. Most reported artificial mimics proteases possess hydrolysis activity under alkaline and high-temperature conditions, which greatly limits their applications in biological systems [11,13,15,40]. In this work, we found $CuFe_2O_4$ has predominant inherent protease-like activity to hydrolyze proteins such as very stable casein and BSA under neutral conditions over a broad temperature range (37–70 °C).

According to the Michaelis-Menten formula and nonlinear regression program, kinetic parameters of protein hydrolyze were calculated. The results show that the affinity of the $CuFe_2O_4$ to the substrate is stronger than that of the majority of the synthetic metalloprotease Cu(II) composites, as well as $CuFe_2O_4$ possessed a higher catalytic activity for BSA and casein. The extremely high catalytic efficiency of natural enzymes is largely dependent on their ability to bring substrates close to their active sites. It has been reported that $CuFe_2O_4$ has some degree of affinity toward acidic amino acid residues, the surface of BSA exposed plenty acidic amino acid residues such as glutamic acid and aspartic acid [41]. Furthermore, $CuFe_2O_4$ itself possesses excellent catalytic properties would be enhanced the hydrolysis activity. For the above reasons, a possible mechanism has been proposed as following:

$$CuFe_2O_4 + BSA \rightarrow BSA - CuFe_2O_4 \rightarrow Hydrolysates$$

The BSA-$CuFe_2O_4$ intermediates produced through interaction between $CuFe_2O_4$ and the acid amino acid residues exposed on the surface of protein, and then activated by the Cu and Fe bimetallic center to hydrolysis of protein into small fragments.

$CuFe_2O_4$ as the first magnetic nanomaterial exhibits high potency to mimic protease activity and hydrolyze proteins under neutral conditions. Considering energy consumption and cost, $CuFe_2O_4$ is more suitable for a large number of industrial production applications. In addition, $CuFe_2O_4$ showed excellent stability, as well as it can be easily separated from the reactants and products with magnets.

In view of the proteases are involved in many pathophysiological processes and various stages of tumor progression, so we evaluated the effect of $CuFe_2O_4$ with protease-like activity on intracellular proteins. Firstly, we focus on the cellular permeability of $CuFe_2O_4$. The good cell permeability will provide opportunities for materials to enter and interact with cells. TEM image showed that the average primary size of $CuFe_2O_4$ was about < 10 nm, which is lower than the size of a small virus (~30 nm). At this small size, $CuFe_2O_4$ could be easily up taken by the mammalian cells (around 10–30 μm) [42]. Secondly, the safety of magnetic $CuFe_2O_4$ was evaluated by measuring the cytotoxicity of different cancer and normal cells, including cancer cells A549, SKOV3, HT-29 and normal cells BABL-3T3 and HUVEC using MTT assay. The results showed that $CuFe_2O_4$ displayed concentration-dependent inhibition in all tested cells and was particularly sensitive against SKOV3 cells. The effect of $CuFe_2O_4$ on SKOV3 was compared with other iron-based and cooper-based materials (Table S3), the IC_{50} of $CuFe_2O_4$ in SKOV3 cells was approximately 10-fold lower than Fe-MIL-100, 30-fold lower than Fe-MIL-88B and 6-fold lower than Fe-MIL-101 after 24 h exposure [43], indicating $CuFe_2O_4$ was even much more effective than iron-based MOF materials (Fe-MIL-101, Fe-MIL-88B and Fe-MIL-100) towards SKOV3 cells under identical condition. Although the IC_{50} of $CuFe_2O_4$ towards SKOV3 cells was higher than that of CQDs/Cu_2O [16], the value of $CuFe_2O_4$ was about 4 times lower than that of Cu-MOF at

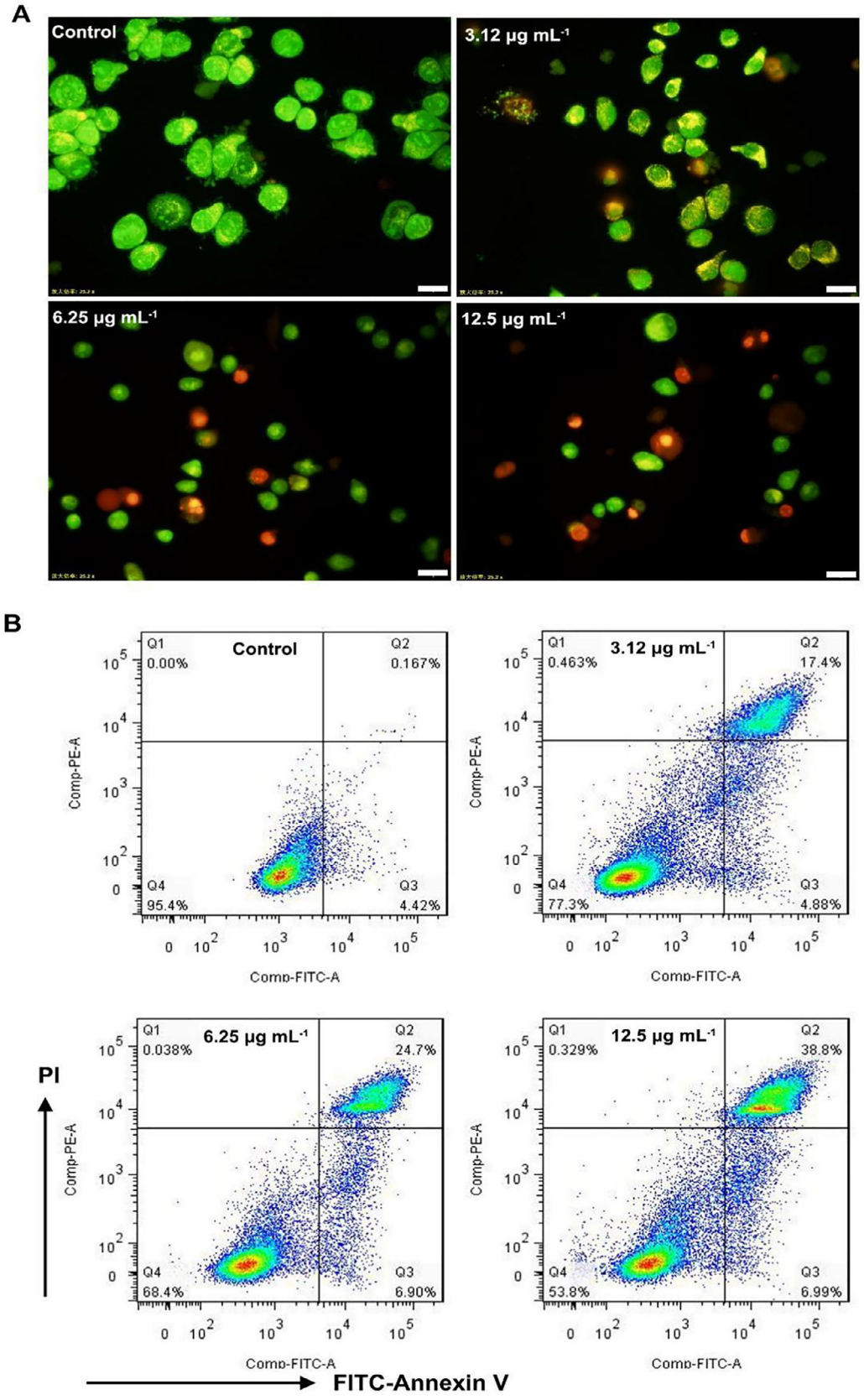

Fig. 3. (A) SKOV3 apoptosis induced by $CuFe_2O_4$ for 24 h. SKOV3 cells were stained by AO/EB. (B) Stained SKOV3 cells with FITC-Annexin-V and PI after 24 h of incubation with $CuFe_2O_4$ (0 ~ 12.5 μg mL^{-1}), and then analysis by flow cytometry.

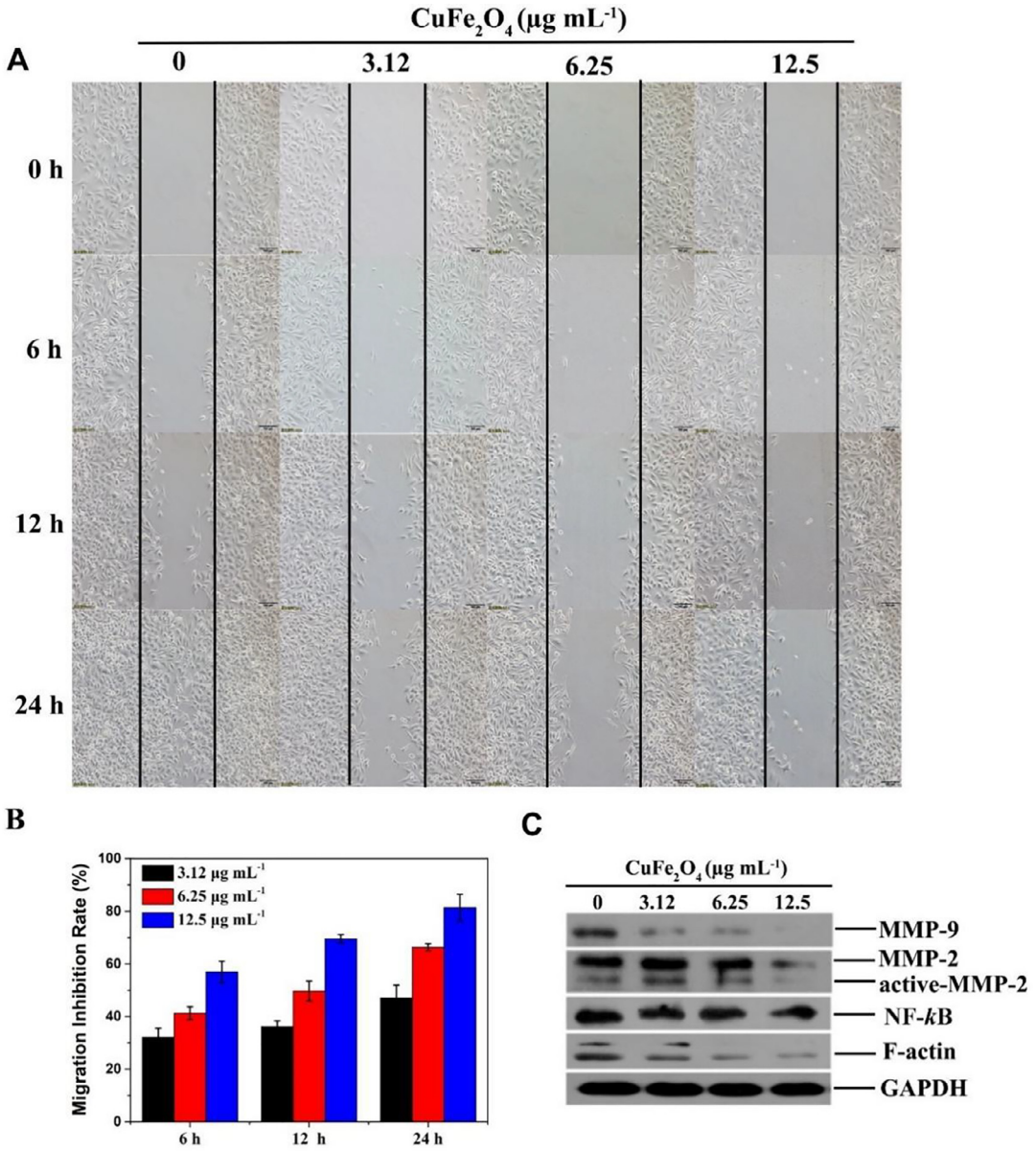

Fig. 4. (A) $CuFe_2O_4$ inhibits migration of SKOV3 cells. Use the pipette tip to make a scratch in the monolayer of cells. (B) The relative migration inhibition rate. (C) MMP-2/9, NF-*k*B and F-actin expression in SKOV3 cells by Western blot. Each experiment is carried out three times, the error is expressed as ± SD.

24 h [31], indicating $CuFe_2O_4$ had a strong inhibitory effect on SKOV3 cell proliferation. The above results indicated that $CuFe_2O_4$ can be used as an effective drug to selectively inhibit SKOV3 cancer cells proliferation. The results of AO/EB staining and annexin V-FITC confirmed $CuFe_2O_4$ effectively induced SKOV3 cell apoptosis.

Local recurrence and metastasis are considered to be the main causes of treatment failure for ovarian cancer [30]. Inhibiting the proliferation and metastasis of cancer cells have become the key to developing effective drugs and therapies. The cell migration inhibition rate and cytotoxicity increased with the increase of the concentration of $CuFe_2O_4$. However, the morphology of SKOV3 cells remained normal and the density did not change significantly. Obviously, the effect of $CuFe_2O_4$ on cell migration was not only dependent on the cytotoxicity. Therefore, the interaction between $CuFe_2O_4$ and cell migration-related proteins was investigated. Matrix metalloproteinases (MMPs), cytoskeleton and transcription factor play an important role in cancer cell growth and metastasis. Gelatinases MMP-2 and MMP-9 promote tumor invasion and metastasis through degrading the extracellular matrix (ECM) [17,18]. Actin, as an important cytoskeleton, maintain cells mechanical strength and regulate cells locomotion [29]. It has been reported the metal-organic frameworks (IRMOF-3) possesses the ability to disrupt F-actin and tubulin, blocking the rat pheochromocytoma cell division [44]. NF- *k*B, a member of Rel transcription factor family, participate in the mediation of many biological activities including inflammation, immune response, cell proliferation, and apoptotic cell death [27,28]. Western blot assay revealed that the expression of migration-related proteins (MMP-2/9 and F-actin) in SKOV3 cells decreased after treated by $CuFe_2O_4$. Moreover, $CuFe_2O_4$ has better MMP-2/9 inhibitory activity than the previously reported $Gd@C_{82}(OH)_{22}$ and HMCN nanoparticles [24,25]. When treated by 12.5 μg mL^{-1} $CuFe_2O_4$, the data of relative densitometric analysis showed a significant difference compared with control group ($P < 0.01$). Down-regulation the expression of these proteins may be caused by global protein hydrolysis, resulting in inhibition of cell migration.

5. Conclusions

Therefore, $CuFe_2O_4$, as a magnetic nanomaterials, has an intrinsic protease-mimic activity to hydrolyze bovine serum albumin (BSA) and casein under physiological conditions, which possess significantly higher catalytic efficiency than other copper nanomaterials and can be recycled for many times. On the other hand, $CuFe_2O_4$ displayed concentration-dependent inhibition in all tested cells (A549, SKOV3, HT-29, BABL-3T3 and HUVEC cells) and was particularly sensitive against SKOV3 cells. $CuFe_2O_4$ mediated the expression of intracellular proteins, such as MMP-2, MMP-9, F-actin, and NF-*k*B, which may be caused by global protein hydrolysis upon $CuFe_2O_4$ treatment, leading to inhibition of cell migration. The result helps to provide a new insight into the relationship between intracellular protein and magnetic materials, and show a promising prospect in tumor therapy.

Declaration of Competing Interest

The authors declare that they have no known competing financial interests or personal relationships that could have appeared to influence the work reported in this paper.

Author Contributions

B. L. and J. W. conceived the idea, supervised all aspects of this project and contributed to the paper and wrote the manuscript. D. C. designed the experiments, carried out the part of experiments and wrote major part of the manuscript. T. L., G. X. and X. Z carried out major part of the experiments. They analyzed the data, was involved in discussions, critical assessment, and manuscript improvements. L. J., L. L. and Y. W. synthesized and characterized the samples. All the authors contributed to the analysis of the data and discussed the manuscript.

Acknowledgements

The authors thank the National Natural Science Foundation of China (81860532), the Yunling Scholar(K264202012420) and Yunnan Applied Basic Research Project s (2018FB013, 202101AT070017). The authors also thank Innovation Team of Yunnan Province and Key Laboratory of Advanced Materials for Wastewater Treatment of Kunming, and the Industrialization Cultivation Project (2016CYH04) from Yunnan Provincial Department of Education for financial support.

The authors also thank Advanced Analysis and Measurement Center of Yunnan University for the sample testing service.

Compliance with ethics guidelines

The authors declare no competing financial interest and no human or animal experiments have been performed.

Supplementary materials

Supplementary material associated with this article can be found, in the online version, at doi:10.1016/j.bbiosy.2021.100038.

References

[1] Ly HGT, Fu G, Kondinski A, et al. Superactivity of MOF-808 toward peptide bond hydrolysis. J Am Chem Soc 2018;140:6325–35.
[2] Loosen A, de Azambuja F, Smolders S, et al. Interplay between structural parameters and reactivity of Zr6-based MOFs as artificial proteases. Chem Sci 2020;11:6662–9.
[3] Wu W, Huang L, Wang E, et al. Atomic engineering of single-atom nanozymes for enzyme-like catalysis. Chem Sci 2020;11:9741–56.
[4] Jiang D, Ni D, Rosenkrans ZT, et al. Nanozyme: new horizons for responsive biomedical applications. Chem Soc Rev 2019;48:3677–998.
[5] Kassai M, Ravi R, Shealy S, et al. Unprecedented acceleration of zirconium(IV)-assisted peptide hydrolysis at neutral pH. Inorg Chem 2004;43:6130–2.
[6] Kim HM, Jang B, Cheon YE, et al. Proteolytic activity of Co(III) complex of 1-oxa-4,7,10-triazacyclododecane: a new catalytic center for peptide-cleavage agents. J Biol Inorg Chem 2009;14:151–7.
[7] Wang X, Wang D, Liang P, et al. Synthesis and properties of an insoluble chitosan resin modified by azamacrocycle copper(II) complex for protein hydrolysis. J Appl Polym Sci 2013;12:83280–8.
[8] Yashiro M, Kawakami Y, Taya JI, et al. Zn(II) complex for selective and rapid scission of protein backbone. Chem Commun 2009;12:1544–6.
[9] Pasquato L, Rancan F, Scrimin P, et al. N-Methylimidazole-functionalized gold nanoparticles as catalysts for cleavage of a carboxylic acid ester. Chem Commun 2000;22:2253–4.
[10] Hegg EL, Burstyn JN. Hydrolysis of unactivated peptide bonds by a macrocyclic copper(II) complex: cu([9]aneN$_3$)Cl$_2$ hydrolyzes both dipeptides and proteins. J Am Chem Soc 1995;117:7015–16.
[11] Kim MG, Yoo SH, Chei WH, et al. Soluble artificial metalloproteases with broad substrate selectivity, high reactivity, and high thermal and chemical stabilities. J Biol Inorg Chem 2010;15:1023–31.
[12] Jeon JW, Son SJ, Yoo CE, et al. Protein-cleaving catalyst selective for protein substrate. Org Lett 2002;4(23):4155–8.
[13] Yoo S, Lee B, Kim H, et al. Artificial metalloprotease with active site comprising aldehyde group and cu(II)cyclen complex. J Am Chem Soc 2005;127:9593–602.
[14] Gao L, Zhuang J, Nie L, et al. Intrinsic peroxidase-like activity of ferromagnetic nanoparticles. Nature Nanotechnol 2007;2:577–83.
[15] Li B, Chen D, Wang J, et al. MOFzyme: intrinsic protease-like activity of Cu-MOF. Sci Rep 2014;4:6759–66.
[16] Li B, Chen D, Nie M, Wang J, et al. Carbon dots/Cu_2O composite with intrinsic high protease-like activity for hydrolysis of proteins under physiological conditions. Particle Particle Systems Characterization 2018;35:1800277–85.
[17] Tang Y, Jaganath IB, Sekaran SD, spp Phyllanthus. induces selective growth inhibition of PC-3 and MeWo human cancer cells through modulation of cell cycle and induction of apoptosis. PlotS One 2010;5:e12644.
[18] Petrova V, Annicchiarico-Petruzzelli M, Melino G, Amelio I. The hypoxic tumour microenvironment. Oncogenesis 2018;7:10.
[19] Liu M, Zhang X, Long C, et al. Collagen-based three-dimensional culture microenvironment promotes epithelial to mesenchymal transition and drug resistance of human ovarian cancer in vitro. RSC Adv 2018;8:8910–19.
[20] Paju A, Sorsa T, Tervahartiala T, et al. The levels of trypsinogen isoenzymes in ovarian tumour cyst fluids are associated with promatrix metalloproteinase-9 but not promatrix metalloproteinase-2 activation. Br J Cancer 2001;84:1363–71.
[21] Ji T, Zhao Y, Ding Y, et al. Using functional nanomaterials to target and regulate the tumor microenvironment: diagnostic and therapeutic applications. Adv Mater 2013;25:3508–25.
[22] Song H, Pan D, Sun W, et al. SiRNA directed against annexin II receptor inhibits angiogenesis via suppressing MMP2 and MMP9 expression. Cellular Physiol Biochem 2015;35:875–84.
[23] Shakibaie M, Haghiri M, Jafari M, et al. Preparation and evaluation of the effect of Fe_3O_4 @ piroctone olamine magnetic nanoparticles on matrix metalloproteinase-2:a preliminary in vitro study. Biotechnol Appl Biochem 2015;61:676–82.
[24] Chen Y, Xu P, Wu M, et al. Colloidal RBC-shaped, hydrophilic, and hollow mesoporous carbon nanocapsules for highly efficient biomedical engineering. Adv Mater 2014;26:4294–301.
[25] Chen C, Xing G, Wang J, et al. Multihydroxylated[$Gd@C_{82}(OH)_{22}$]$_n$ nanoparticles: antineoplastic activity of high efficiency and low toxicity. Nano Lett 2005;5:2050.
[26] Sun PJ, Lee KE, Jung YD. Cadmium stimulates urokinase plasminogen activator receptor expression via ROS and Erk-1/2 pathway through NF-kB and AP-1 Signaling in human gastric cancer cells. Eur J Cancer 2012;48:S164.
[27] Dejardin E, Deregowski V, Chapelier M, et al. Regulation of NF-κB activity by IκB-related proteins in adenocarcinoma cells. Oncogene 1999;18(16):2567–77.
[28] Bours V, Dejardin E, Goujon-Letawe F, et al. The NF-κB transcription factor and cancer: high expression of NF-κB-and IκB-related proteins in tumor cell lines. Biochem Pharmacol 1994;47:145–9.
[29] Caporizzo MA, Sun Y, Goldman YE, Composto RJ. Nanoscale topography mediates the adhesion of F-actin. Langmuir 2012;28:12216–24.
[30] Chen D, Li B, Lei T, et al. Selective mediation of ovarian cancer SKOV3 cells death by pristine carbon quantum dots/Cu_2O composite through targeting matrix metalloproteinases, angiogenic cytokines and cytoskeleton. J Nanobiotechnology 2021;19(1):1–17.
[31] Chen D, Li B, Jiang Liang, et al. Pristine Cu-MOF induces mitotic catastrophe and alterations of gene expression and cytoskeleton in ovarian cancer cells. ACS Appl Bio Mater 2020;3(7):4081–94.
[32] Yang Z, Ma F, Zhu Y, et al. A facile synthesis of $CuFe_2O_4$/Cu_9S_8/PPy ternary nanotubes as peroxidase mimics for the sensitive colorimetric detection of H_2O_2 and dopamine. Dalton Trans 2017;46:11171–9.
[33] Xia F, Shi Q, Nan Z. Facile synthesis of Cu-$CuFe_2O_4$ nanozymes for sensitive assay of H_2O_2 and GSH. Dalton Trans 2020;49:12780–92.
[34] Su L, Feng J, Zhou X, et al. Colorimetric detection of urine glucose based $ZnFe_2O_4$ magnetic nanoparticles. Anal Chem 2012;84(13):5753–8.
[35] Su L, Qin W, Zhang H, et al. The peroxidase/catalase-like activities of MFe_2O_4 (M= Mg, Ni, Cu) MNPs and their application in colorimetric biosensing of glucose. Biosens Bioelectron 2015;63:384–91.
[36] He F, Li W, Zhao F, et al. Pt deposited on magnetic $CoFe_2O_4$ nanoparticles: double enzyme-like activity, catalytic mechanism and fast colorimetric sensing of dopamine. Microchem J 2020;158:105264.
[37] Xian Z, Zhang L, Yu Y, et al. Nanozyme based on $CoFe_2O_4$ modified with MoS_2 for colorimetric determination of cysteine and glutathione[J]. Microchimica Acta, 2021;188(3):1–9.
[38] Guo Y, Zhang L, Liu X, Li B, et al. Synthesis of magnetic core–shell carbon dot@MFe_2O_4 (M=Mn, Zn and Cu) hybrid materials and their catalytic properties. J Mater Chem A 2016;4:4044–55.

[39] Liu Y, Niu Z, Lu Y, et al. Facile synthesis of $CuFe_2O_4$ crystals efficient for water oxidation and H_2O_2 reduction. J Alloys Compd 2018;735:654–9.
[40] Jang SW, Suh J. Proteolytic activity of Cu(ii) complex of 1-oxa-4,7,10-triazacyclododecane. Org Lett 2008;10:481.
[41] Zheng J, Lin Z, Liu W, et al. One-pot synthesis of $CuFe_2O_4$ magnetic nanocrystal clusters for highly specific separation of histidine-rich proteins. J Mater Chem B 2014;2(37):6207–14.
[42] Chia SL, Tay CY, Setyawati MI, et al. Decoupling the direct and indirect biological effects of ZnO nanoparticles using a communicative dual cell-type tissue construct. Small 2016;12(5):647–57.
[43] Wang J, Chen D, Li B, et al. Fe-MIL-101 exhibits selective cytotoxicity and inhibition of angiogenesis in ovarian cancer cells via downregulation of MMP. Sci Rep 2016;6:26126.
[44] Ren F, Yang B, Cai J, et al. Toxic effect of zinc nanoscale metal-organic frameworks on rat pheochromocytoma (PC12) cells in vitro. J Hazard Mater 2014;271:283–91.